Fortilin binds Ca^{2+} and blocks Ca^{2+}-dependent apoptosis *in vivo*

Potchanapond GRAIDIST*†, Michio YAZAWA‡, Moltira TONGANUNT†§, Akiko NAKATOMI‡, Curtis Chun-Jen LIN†, Jui-Yoa CHANG†, Amornrat PHONGDARA§ and Ken FUJISE†‖¶[1]

*Department of Biomedical Sciences, Faculty of Medicine, Prince of Songkla University, Hat-Yai, Songkhla, Thailand, 90110, †Brown Foundation Institute of Molecular Medicine for the Prevention of Human Diseases, Houston, TX 77030, U.S.A., ‡Faculty of Advanced Life Science, Division of Cellular Life Science, Hokkaido University, Sapporo, Japan, 060-0810, §Center for Genomics and Bioinformatics Research, Faculty of Science, Prince of Songkla University, Hat-Yai, Songkhla, Thailand, 90112, ‖Division of Cardiology, Department of Internal Medicine, Medical School, University of Texas Health Science Center at Houston, Houston, TX 77030, U.S.A., and ¶St. Luke's Episcopal Hospital, Houston, TX 77030, U.S.A.

Fortilin, a 172-amino-acid polypeptide present both in the cytosol and nucleus, possesses potent anti-apoptotic activity. Although fortilin is known to bind Ca^{2+}, the biochemistry and biological significance of such an interaction remains unknown. In the present study we report that fortilin must bind Ca^{2+} in order to protect cells against Ca^{2+}-dependent apoptosis. Using a standard Ca^{2+}-overlay assay, we first validated that full-length fortilin binds Ca^{2+} and showed that the N-terminus (amino acids 1–72) is required for its Ca^{2+}-binding. We then used flow dialysis and CD spectropolarimetry assays to demonstrate that fortilin binds Ca^{2+} with a dissociation constant (K_d) of approx. 10 μM and that the binding of fortilin to Ca^{2+} induces a significant change in the secondary structure of fortilin. In order to evaluate the impact of the binding of fortilin to Ca^{2+} *in vivo*, we measured intracellular Ca^{2+} levels upon thapsigargin challenge and found that the lack of fortilin in the cell results in the exaggerated elevation of intracellular Ca^{2+} in the cell. We then tested various point mutants of fortilin for their Ca^{2+} binding and identified fortilin(E58A/E60A) to be a double-point mutant of fortilin lacking the ability of Ca^{2+}-binding. We then found that wild-type fortilin, but not fortilin(E58A/E60A), protected cells against thapsigargin-induced apoptosis, suggesting that the binding of fortilin to Ca^{2+} is required for fortilin to protect cells against Ca^{2+}-dependent apoptosis. Together, these results suggest that fortilin is an intracellular Ca^{2+} scavenger, protecting cells against Ca^{2+}-dependent apoptosis by binding and sequestering Ca^{2+} from the downstream Ca^{2+}-dependent apoptotic pathways.

Key words: apoptosis, Ca^{2+}, cell death, fortilin, thapsigargin.

INTRODUCTION

Fortilin is a 172-amino-acid polypeptide originally identified in our laboratory as a molecule that specifically interacts with MCL1 (myeloid cell leukaemia sequence 1) [1], a member of the Bcl-2 family of anti-apoptotic molecules [2]. Fortilin is also known as TCTP (translationally controlled tumour protein).

The amino acid sequence of fortilin is highly conserved among species ranging from human to rice [3]. Its message is distributed ubiquitously in normal tissue, most abundantly in the liver and kidney [3]. Fortilin is present in both the nucleus and cytosol [3], inducible by serum stimulation [4] and heavy metals [5], and expressed at much higher levels in cancerous cell lines than in non-cancerous cell lines [3]. Fortilin is overexpressed in a variety of human malignancies, including liver, thyroid, laryngeal, skin, uterine, breast, ovarian, prostate and rectal cancers [6]. Fortilin has a potent anti-apoptotic function: its overexpression protects HeLa [3] and U2OS [7] cells against apoptosis. In addition, the depletion of fortilin from cells induces spontaneous cell death in MCF-7 [3] and U937 cells [6]. Although fortilin is likely to make cells cancerous and cancerous cells more resistant to chemotherapy by preventing these cells from undergoing apoptosis, the exact mechanism by which fortilin blocks apoptosis remains unknown.

That fortilin binds calcium was originally shown by Haghighat and Ruben in 1992 [8]. In that work, a large quantity of homogenate of *Trypanosoma brucei*, the parasitic cause of West African sleeping sickness, was fractionated and probed by $^{45}Ca^{2+}$ in a Ca^{2+}-overlay assay to identify Ca^{2+}-binding proteins. One of the proteins shown by the Ca^{2+}-overlay assay to bind Ca^{2+} was a 22-kDa protein, whose N-terminal sequence was found to be identical with that of *T. brucei* fortilin [8]. The fact that fortilin binds Ca^{2+} has since been validated by Ca^{2+}-overlay assays in several laboratories including those of Sanchez et al. [9], Kim et al. [10], Rao et al. [11] and Arcuri et al. [12]. In 1999, Xu et al. [13] reported that Ca^{2+} up-regulated fortilin transcription, suggesting a role for fortilin in intracellular calcium homoeostasis. However, the biochemistry of the fortilin–Ca^{2+} interaction has not been extensively studied. In addition, the exact biological consequence of fortilin binding to Ca^{2+} remains unknown. Furthermore, it is unknown whether fortilin is required to bind Ca^{2+} in order to block the Ca^{2+}-dependent apoptosis.

The cytosolic concentration of free Ca^{2+} is maintained at very low levels (~100 nM) by the continuous pumping of Ca^{2+} out of the cytosol into the ER (endoplasmic reticulum) by SERCAs (sarcoplasmic/endoplasmic reticulum Ca^{2+}-ATPases) [14]. This explains why the ER, among all organelles, contains the highest concentration of Ca^{2+} and why the inhibition of SERCAs, for example by thapsigargin, immediately and drastically elevates Ca^{2+} levels in the cytosol. Even slight elevation of the Ca^{2+} concentration beyond the tightly regulated range could lead to the most drastic biological phenotype, death of the cell by apoptosis. Cytosolic Ca^{2+} beyond the normal range could attack and injure mitochondrial membranes, leading to the release of pro-apoptotic molecules such as cytochrome *c* and AIF

Abbreviations used: AM, acetoxymethyl; BAPTA-AM, acetoxy-methyl-1,2-bis(2-aminophenoxy)ethane-N,N,N′,N′-tetraacetic acid; CBB, Ca^{2+}-binding buffer; DMEM, Dulbecco's modified Eagle's medium; EDB, equilibrium dialysis buffer; ER, endoplasmic reticulum; EthD-1, ethidium homodimer-1; FCS, fetal calf serum; GST, glutathione transferase; MEF, mouse embryonic fibroblast; R110, benzyloxycarbonyl-DEVD-rhodamine 110; r-$[Ca^{2+}]_{i\text{-}base}$, baseline relative intracellular Ca^{2+} concentration; RFI, relative fluorescence intensity; RFU, relative fluorescence unit; SERCA, sarcoplasmic/endoplasmic reticulum Ca^{2+}-ATPase; siRNA, small-interfering RNA.

[1] To whom correspondence should be addressed (email Kenichi.Fujise@uth.tmc.edu).

(apoptosis-inducing factor) [14,15], and to programmed cell death. Ca^{2+} can also induce apoptosis by activating pro-apoptotic Ca^{2+}–CaM-dependent enzymes [16–18], Ca^{2+}-dependent endonucleases [19], Ca^{2+}-binding cysteine proteases [20–22], calcineurin [23] and Ca^{2+}-sensitive NO synthases [14,24]. Once Ca^{2+} levels go beyond a critical threshold to activate one of these death-bound pathways, apoptosis is inevitable.

It is possible, however, that there is a cellular mechanism by which the cell sequesters cytosolic Ca^{2+} before it activates the downstream cell-death pathways described above. Based on the fact that fortilin blocks apoptosis [3] and the fact that fortilin binds Ca^{2+}[8], we hypothesized that fortilin binds Ca^{2+} in the cytosol, functions as a Ca^{2+} scavenger and sequesterer, prevents Ca^{2+} levels from going beyond the apoptosis threshold and protects cells against Ca^{2+}-dependent cell death. We hypothesized that the anti-apoptotic activity of fortilin was due to its binding to, and consequent sequestration from downstream apoptotic pathways of, Ca^{2+} that was released in response to apoptotic stimuli. In the present study we report that fortilin indeed binds Ca^{2+} and scavenges Ca^{2+} released in response to thapsigargin, preventing cytosolic Ca^{2+} levels from increasing and activating Ca^{2+}-dependent apoptosis pathways.

MATERIALS AND METHODS

Materials

Calmodulin was a gift from Dr John A. Patkey (The University of Texas Health Science Center at Houston, Houston, TX, U.S.A.). Fortilin peptides were chemically synthesized by GenScript. The sequence of each peptide is shown in Figure 8(A). For all procedures described below, plastic and glass instruments were rinsed several times with 0.1 M HCl and then washed extensively with ultra-pure water to remove contaminating Ca^{2+}.

Molecular cloning

The cDNA of fortilin and its deletion and point mutants were synthesized by PCR-based strategies as we have described previously [25]. In all cases, the authenticity of cloned constructs was confirmed by automated dideoxynucleotide sequencing (Lark Technologies).

Expression and purification of recombinant fortilin and its mutants

Expression and purification of recombinant fortilin protein and its mutants were performed as previously described [26], using *Escherichia coli* BL21 cells transfected with pGEX-fortilin (or its mutants; Amersham–Pharmacia) or pQE41-fortilin (Qiagen).

Ca^{2+}-overlay assay

Ca^{2+}-overlay assays were performed as described previously [9,10,12,13,27]. In brief, proteins were size-fractionated by SDS/PAGE and transferred on to a PVDF membrane (Immobilon-P). The membrane was air-dried, incubated for 2 h at room temperature (25 °C) with $^{45}CaCl_2$ (MP Biomedicals) in CBB [Ca^{2+}-binding buffer; 60 mM KCl, 5 mM $MgCl_2$ and 10 mM imidazole (pH 6.8)] at a final concentration of 40 μCi/ml, rinsed in CBB, washed in 50 % ethanol for 10 min, air-dried, and exposed to a phosphor imager screen overnight. Signals were detected by a Molecular Scanner-FX and Quantity One software system (Bio-Rad), according to the manufacturer's instructions. Proteins transferred on to the membrane were semi-quantitatively assessed by Ponceau S staining.

CD spectropolarimetry

Far-UV CD spectra of GST (glutathione transferase)–fortilin samples (0.36 μg/μl) were collected on a Jasco J715 spectropolarimeter using a 1-mm-path-length quartz cuvette at room temperature. Spectra were recorded from 260 to 195 nm in 0.5 nm steps at 100 nm/min. Data represent the average of 10 independent spectra. All protein samples were passed through a PD-10 column (Sephadex-25; Pharmacia) equilibrated in 0.1 M phosphate buffer (pH 7.4) for desalting. The samples were then passed twice through a Chelex 100 chelating ion-exchange resin column (Bio-Rad). Data were expressed as mean residue ellipticity (degrees cm^2/dmol).

Flow dialysis assay

A flow dialysis assay was performed as previously described [28], at 25 °C, using $^{45}CaCl_2$ and Spectrapore 6 cellulose dialysis membrane (M_r cut-off 1000 Da, Spectrum Medical Industry). The flow rate was 3 ml/min and the response time of the apparatus was about 0.9 min. Initially, 2.25 μCi of $^{45}Ca^{2+}$ was added into 1 ml of the GST–fortilin protein solution in the upper chamber. After the successive titration with unlabelled Ca^{2+}, an 800 μl portion of the dialysate fraction (1 ml/tube) which flowed out through the lower chamber (0.66 ml) was taken, and the radioactivity was determined using a Beckmann LS-600C liquid scintillation counter. The resulting Ca^{2+}-binding data were analysed by fitting to the Adair equation for the 2-site model:

$$y = (x/K_1 + 2x^2/K_1/K_2)/(1 + x/K_1 + x^2/K_1/K_2)$$

where y is the number of bound Ca^{2+} (mol/mol-protein), x is the concentration of free Ca^{2+} and K_1 and K_2 are the macroscopic dissociation constants.

Cell, cell lines and culture conditions

U2OS cells and MEFs (mouse embryonic fibroblasts) were maintained in DMEM (Dulbecco's modified Eagle's medium) supplemented with 10 % FCS (fetal calf serum) and, when appropriate, antibiotics. MEF cells from passages 4–9 were used in all experiments.

Isolation of MEFs

MEFs were isolated as previously described [29–31].

Western blot analysis

Cells were harvested by the direct addition of Laemmli SDS gel loading buffer [1,3]. When appropriate, cells were harvested into RIPA buffer [50 mM Tris/HCl (pH 7.4), 150 mM NaCl, 1 % NP40 (Nonidet P40), 0.1 % SDS, 0.5 % sodium deoxycholate, and protease inhibitors (Complete Protease Inhibitor Cocktail Tablets; Roche Biochemicals)] for the determination of protein concentrations (using the Bradford method; Bio-Rad). Western blot analysis was performed as described previously [3,25], using anti-fortilin and anti-actin (Roche Molecular Biochemicals) antibodies.

In vivo Ca^{2+} release assay

U2OS (1×10^4) or MEF (2×10^4) cells were seeded in each well of a 96-well plate. The next day, the cells were transfected with either siRNA (small interfering RNA) against luciferase, a non-mammalian protein from *Photinus pyralis* (American firefly) ($siRNA_{luciferase}$, control), or siRNA against human fortilin ($siRNA_{fortilin}$) at final concentrations of 100 nM. Both siRNAs [32,33] were synthesized by Dharmacon Research.

Transfection was carried out using the DharmaFECT™ two transfection reagent (Dharmacon) as described previously [1]. The $siRNA_{fortilin}$ consisted of a mixture of four siRNA duplexes targeting four different regions of fortilin mRNA, namely 5′-AGATGTTCTCCGACATCTA-3′, 5′-CGAAGGTACCGAAAGCACA-3′, 5′-GGGAGATCGCGGACGGGTT-3′ and 5′-GGTACCGAAAGCACAGTAA-3′. At 48 h after transfection, cells were exposed to 5 μM Fura 2/AM (fura 2 acetoxymethyl ester) for 1 h at 37 °C under 5 % CO_2, allowed to recover in DMEM with 10 % FCS for 20 min, and transferred to assay buffer consisting of HBSS (Hanks balanced salt solution; Cambrex Bioscience) supplemented with 10 mM Hepes, 200 μM Ca^{2+}, 0.1 % BSA, 2.5 mM probenecid and pluronic-F127 (Molecular Probes). A baseline relative intracellular Ca^{2+} concentration (termed r-$[Ca^{2+}]_{i\text{-base}}$), was calculated by first obtaining a fluorescent signal by excitation at 355 nm and emission at 505 nm [termed $RFU_{355/505}$ (where RFU is the relative fluorescence unit)] and a fluorescent signal by excitation at 363 nm and emission at 512 nm (termed $RFU_{363/512}$) on a SpectraMax M2 plate reader (Molecular Probes) and then dividing $RFU_{355/505}$ by $RFU_{363/512}$, as described previously [34]. The Fura 2 fluorescence emission ratio [i.e. the ratio of RFI (relative fluorescence intensity) at an excitation at 355 nm and an emission at 505 nm ($RFI_{355/505}$) to an excitation at 363 nm and emission at 512 nm ($RFI_{363/512}$)] correlates with intracellular Ca^{2+} concentration ($[Ca^{2+}]_i$) [34]. At zero time, thapsigargin (Sigma) was added to a final concentration of 400 nM. Then, fluorescent signals ($RFU_{355/505}$ and $RFU_{363/512}$) were obtained every 10 s for the next 10 min. The r-$[Ca^{2+}]_i$ at a given time point was calculated by dividing $RFU_{355/505}$ by $RFU_{363/512}$ minus r-$[Ca^{2+}]_{i\text{-base}}$. The free intracellular Ca^{2+} index represents the area under the curve between zero time and 600 s and was expressed as an arbitrary unit. Thapsigargin, a sesquiterpene γ-lactone derived from the plant *Thapsia garganica*, is a specific and irreversible inhibitor of the SERCAs, including SERCA1, SERCA2a, SERCA2b and SERCA3 [35]. Conversely, thapsigargin has no effect on plasma membrane Ca^{2+}-ATPase, Na,K-ATPase, or other enzymes [35]. In addition, the administration of thapsigargin results in the immediate and drastic elevation of $[Ca^{2+}]_i$ [36]. Experiments were performed in quadruplicate and repeated at least three times, with consistent results. After the determination of r-$[Ca^{2+}]_i$, cells were subjected to Western blot analysis as described above.

Cell death assay in the presence and absence of BAPTA-AM [acetoxy-methyl-1,2-bis(2-aminophenoxy)ethane-N,N,N′,N′-tetraacetic acid]

In brief, 1.5×10^4 U2OS cells were seeded in each well of a 96-well plate and transfected with $siRNA_{fortilin}$ or $siRNA_{luciferase}$ as described above. A cell death assay using EthD-1 (ethidium homodimer-1; Molecular Probes) was performed as described previously [37,38], with the following modifications. At 12 h after transfection, cells were treated with 15 μM BAPTA-AM-Ca^{2+}-chelator (Molecular Probe) or vehicle (DMSO) for 45 min at 37 °C, washed twice with PBS, challenged with 1 μM thapsigargin or vehicle, and incubated for 18 h at 37 °C. After incubation, cells were washed with PBS and stained with 8 μM EthD-1 for 30 min at room temperature. EthD-1 is excluded from living cells but can cross the compromised plasma and nuclear membranes of dying cells and interact with nucleic acids to give red fluorescence. EthD-1 positivity has been observed in the late-phase of apoptosis or in necrosis [37,38]. Fluorescent signals were obtained by 528 nm excitation and 617 nm emission ($RFU_{528/617}$). The EthD-1 index, reflecting cell death rate, was calculated using the following equation:

$$([RFU_{528/617}] - [RFU_{528/617}]_{TG0})/([RFU_{528/617}]_{saponin} - [RFU_{528/617}]_{TG0}) \times 100$$

where $[RFU_{528/617}]_{TG0}$ is the $RFU_{528/617}$ from non-TG-treated cells (background) and $[RFU_{528/617}]_{saponin}$ is $RFU_{528/617}$ from cells treated with 0.1 % saponin (Sigma). Typically, EthD-1 indices were calculated for two groups of cells, one treated and one not treated with BAPTA-AM. The EthD-1 indices of BAPTA-AM-treated cells represented Ca^{2+}-independent cell death rates, whereas those of non-BAPTA-AM-treated cells represented total cell death rates both Ca^{2+}-dependent and -independent. Data from caspase 3 activity assays (Figures 6C and 7C) show that most of thapsigargin-induced Ca^{2+}-dependent cell death represents necrosis, without significant activation of caspase 3. For MEF, 1.5×10^4 $MEF_{fortilin+/-}$ or $MEF_{fortilin+/+}$ cells were used. Experiments were normally performed in quadruplicate and repeated at least three times, with consistent results.

Caspase 3 activity assay

Caspase 3 assays for MEFs and siRNA-treated U2OS cells were performed as previously described [3]. In brief, cells were treated with 1 μM thapsigargin or vehicle as described above. Cytosolic proteins were extracted by three cycles of freezing and thawing in hypotonic cell lysis buffer [25 mM Hepes (pH 7.5), 5 mM $MgCl_2$, 5 mM EDTA, 5 mM dithiothreitol and 0.05 % PMSF; all from Sigma]. Cytosolic extracts (20 μg) were added to caspase assay buffer [312.5 mM Hepes (pH 7.5), 31.25 % sucrose and 0.3125 % CHAPS] with R110 (benzyloxycarbonyl-DEVD-rhodamine 110) as substrates (Molecular Probes). Release of R110 by caspase-3-like activity was quantified, after 2 h of incubation at 37 °C, using a SpectraMax M2 plate reader (Molecular Probes) set to an excitation value of 498 nm and emission value of 521 nm. The results were expressed as relative fluorescence units/μg of protein.

Equilibrium dialysis assay of fortilin peptides and GST–fortilin and its mutants

An equilibrium dialysis assay to assess qualitatively the binding of candidate proteins and peptides to Ca^{2+} was performed as described previously [39–41], with modifications. Briefly, 100 μl each of fortilin peptides, GST, GST–fortilin, its mutants or His_6-tagged fortilin [20 μM in EDB (equilibrium dialysis buffer; 10 mM Mops, pH 7.4 and 100 mM KCl)] was placed in a Tube-O-Dialyzer tube (M_r cut off 1000 Da; Genotech), which was then placed in a beaker containing 200 ml of EDB with 1 μM Ca^{2+} and $^{45}Ca^{2+}$ at 1000 c.p.m./μl. The radioactivity of each 15 μl aliquot was determined in triplicate.

Generation of cells stably overexpressing fortilin and its mutant

U2OS cells were transfected, using FuGENE™ 6 reagent (Roche Molecular Biochemicals), with empty pcDNA4-His-Max (pcDNA4; Invitrogen) or pcDNA4 containing the cDNA encoding either wild-type fortilin ($pcDNA4_{Fortilin}$) or its mutant ($pcDNA4_{Fortilin\Delta2}$). FortilinΔ2 contained two point mutations: the glutamate residues at amino acid positions 58 and 60 were both mutated to alanine residues and sometimes referred to as fortilin(E58A/E60A). Transfected cells were selected in medium containing 400 μg/ml Zeocin (Invitrogen) and characterized by Western blot analyses. The resulting cell lines were named $U2OS_{empty}$, $U2OS_{fortilin}$ and $U2OS_{fortilin\Delta2}$ respectively.

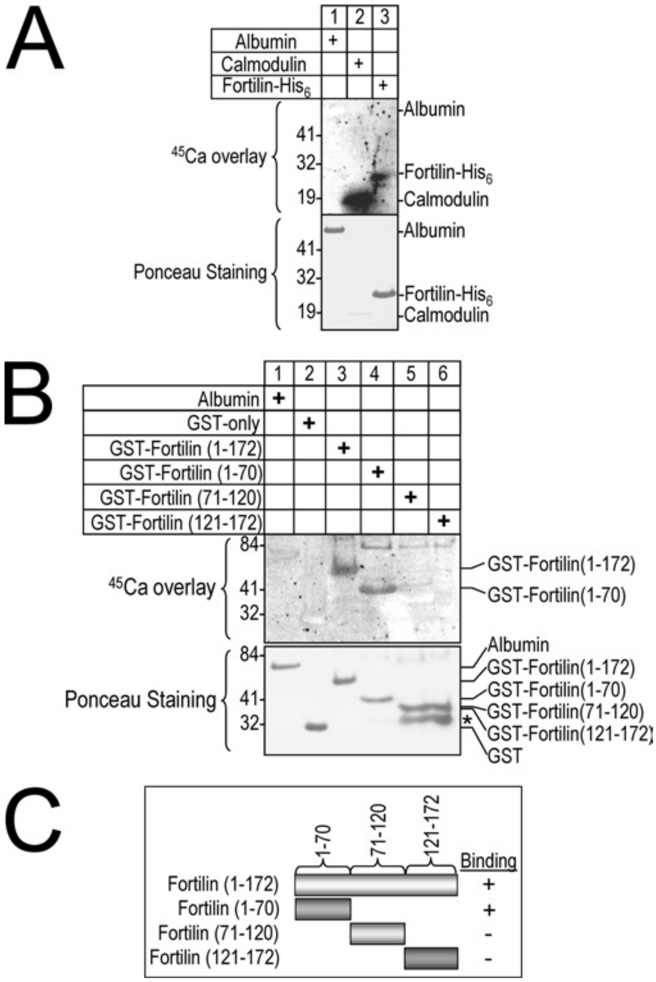

Figure 1 Ca^{2+}-overlay assay shows that fortilin binds Ca^{2+} through its first 70 amino acids

(**A**) Ca^{2+}-overlay assay of fortilin–His$_6$. (**B**) Ca^{2+}-overlay assay of GST–fortilin and its deletion mutants. Exactly 10 μg of proteins were size-fractionated by SDS/PAGE and transferred on to a PVDF membrane, which was then incubated with $^{45}Ca^{2+}$, washed and exposed to a phosphor imager screen. Neither albumin nor GST-only bound Ca^{2+}, whereas calmodulin (a known Ca^{2+}-binding protein) did bind Ca^{2+}. In this system, both fortilin–His$_6$ (**A**) and GST–fortilin (**B**) bound Ca^{2+}. In addition, GST–fortilin(1–70), but not GST–fortilin(71–120) or GST–fortilin(121–172), bound Ca^{2+} (**B** and **C**). *Degradation products.

Statistical analysis

Experiments were performed in duplicate, triplicate or quadruplicate to obtain S.D. Variations in flow dialysis were expressed as S.E.M. Differences between two experimental groups were analysed using the Student's t test. $P < 0.05$ was considered statistically significant.

RESULTS

Fortilin binds Ca^{2+} in a Ca^{2+}-overlay assay

To test the hypothesis that fortilin binds to Ca^{2+}, standard Ca^{2+}-overlay assays were performed where proteins of interest were resolved by SDS/PAGE and transferred on to PVDF membranes, which were in turn incubated with $^{45}Ca^{2+}$, washed and exposed to a phosphor imager screen. As shown in Figure 1(A), $^{45}Ca^{2+}$ was not bound at all by albumin (lane 1), was bound robustly by the established Ca^{2+}-binding protein calmodulin (lane 2), and was bound by fortilin–His$_6$ (lane 3). Using the same system, we tested different portions of fortilin for their importance in Ca^{2+} binding. As shown in Figure 1(B), full-length fortilin [GST–fortilin(1–172)], but not BSA or GST alone, bound $^{45}Ca^{2+}$ (lane 3 compared with lanes 1 and 2). In this system, GST–fortilin(1–70), but not GST–fortilin(71–120) or GST–fortilin(121–172), bound $^{45}Ca^{2+}$. These results suggest that fortilin in fact binds Ca^{2+} and that the 70 amino acid residues at the N-terminus of fortilin are critical for the binding of fortilin to Ca^{2+} (Figure 1C).

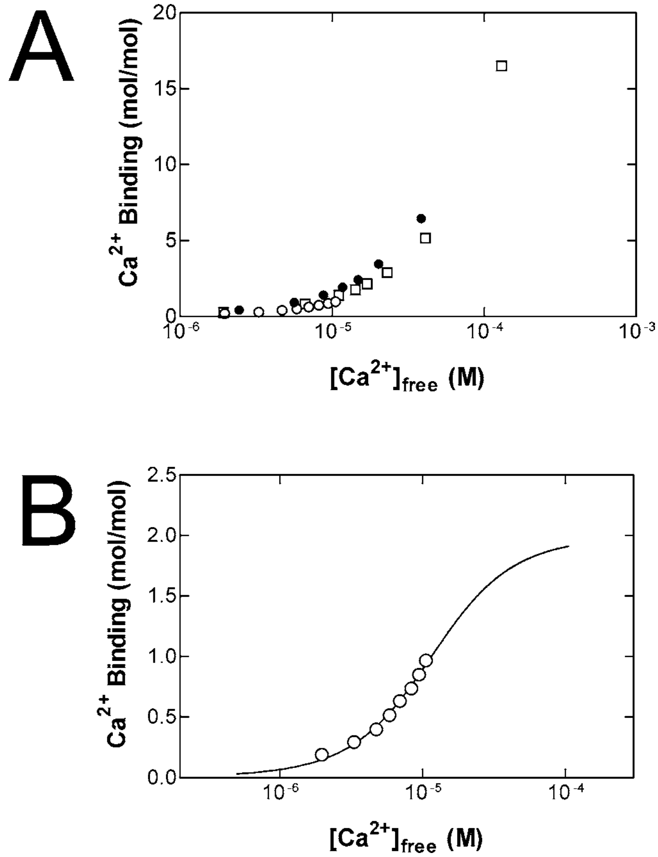

Figure 2 Flow dialysis confirms that fortilin binds Ca^{2+}

(**A**) Ca^{2+} binding to GST–fortilin. Ca^{2+} binding was measured at 25 °C by flow dialysis as described in the Materials and methods section. The results of three independent experiments were shown. Concentrations of GST–fortilin were 24.7 μM (○), 18.4 μM (□) and 13.8 μM (●) in 0.1 M NaCl and 20 mM Mops/NaOH (pH 7.0). (**B**) Ca^{2+} binding to the high-affinity sites of fortilin. One of the results in (**A**) (24.7 μM GST–fortilin) was quantitatively analysed by fitting to an Adair equation (see the Materials and methods section) revealing two Ca^{2+}-binding sites with $K_1 = 1.75 \times 10^{-5}$ M ($\pm 3.06 \times 10^{-6}$ M) and $K_2 = 7.58 \times 10^{-6}$ M ($\pm 1.64 \times 10^{-6}$ M).

Flow dialysis assays suggest the presence of two high-affinity Ca^{2+}-binding sites in fortilin

In order to characterize further the binding of fortilin to Ca^{2+}, flow dialysis assays were performed. Results of three independent measurements were shown in Figure 2(A). GST–fortilin showed a biphasic Ca^{2+} binding, binding to approx. two sites with high affinity and to multiple sites with lower affinity. The high-affinity sites were almost saturated at approx. 10 μM Ca^{2+}. Ca^{2+} binding to the lower-affinity sites disturbed the measurement of the high-affinity sites and the Ca^{2+}-binding data to the latter were scattered. One of the three experimental results was less scattered in this range, and was subjected to curve-fitting analysis (Figure 2B), which revealed two high-affinity sites with macroscopic dissociation constants of $K_1 = 1.75 \times 10^{-5}$ M

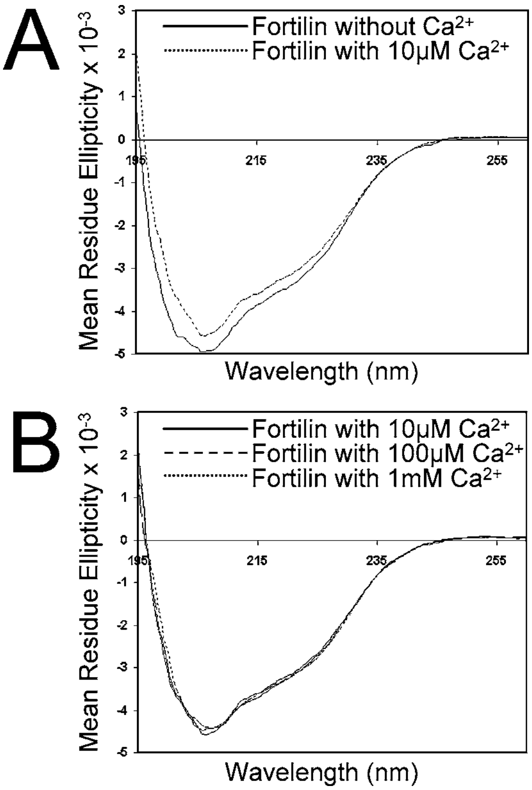

Figure 3 The binding of fortilin to Ca^{2+} changes its secondary structure as assessed by CD spectra

Far-UV CD spectra of GST–fortilin (0.36 mg/ml each) in the presence of no Ca^{2+} and 10 μM, 100 μM, and 1 mM Ca^{2+}, were collected and recorded from 260 to 200 nm in 0.5-nm steps at 100 nm/min. The samples had been passed through a Chelex 100 chelating ion-exchange resin column (Bio-Rad) to remove residual Ca^{2+} from samples. Data are expressed as mean residue ellipticity (degrees cm^2/dmol). The CD spectra of fortilin changed in the presence of 10 μM Ca^{2+} (**A**) but changed no further at Ca^{2+} concentrations greater than 10 μM (**B**), suggesting that Ca^{2+}-binding sites on fortilin were saturated by approx. 10 μM Ca^{2+}.

($\pm 3.06 \times 10^{-6}$ M) and $K_2 = 7.58 \times 10^{-6}$ M ($\pm 1.64 \times 10^{-6}$ M). Although the exact nature of the Ca^{2+} binding to the low-affinity sites is not clear from these experiments, these results again suggest that fortilin binds Ca^{2+} and that there are two high-affinity binding sites with dissociation constants of 7.58 and 17.5 μM.

Fortilin changes its secondary structure in the presence of Ca^{2+}

To determine whether fortilin changes its secondary structure in the presence of Ca^{2+}, we subjected fortilin–His_6 to CD spectropolarimetry analyses in the absence and presence of Ca^{2+}. As shown in Figure 3(A), fortilin did change its secondary structure in the presence of 10 μM Ca^{2+}, most significantly at a wavelength of ~200 nm. More important, the secondary structure of fortilin remained the same in the presence of 10 μM, 100 μM and 1 mM Ca^{2+}, suggesting that Ca^{2+} saturated fortilin at concentrations of approx. 10 μM or greater (Figure 3B). In addition to the fact that the CD spectrum change again suggests the presence of an interaction between fortilin and Ca^{2+}, these results also suggest that the dissociation constant (K_d) of the fortilin–Ca^{2+} interaction is in the vicinity of 10 μM (Figures 3A and 3B), a finding that is consistent with the flow dialysis data (Figure 2B).

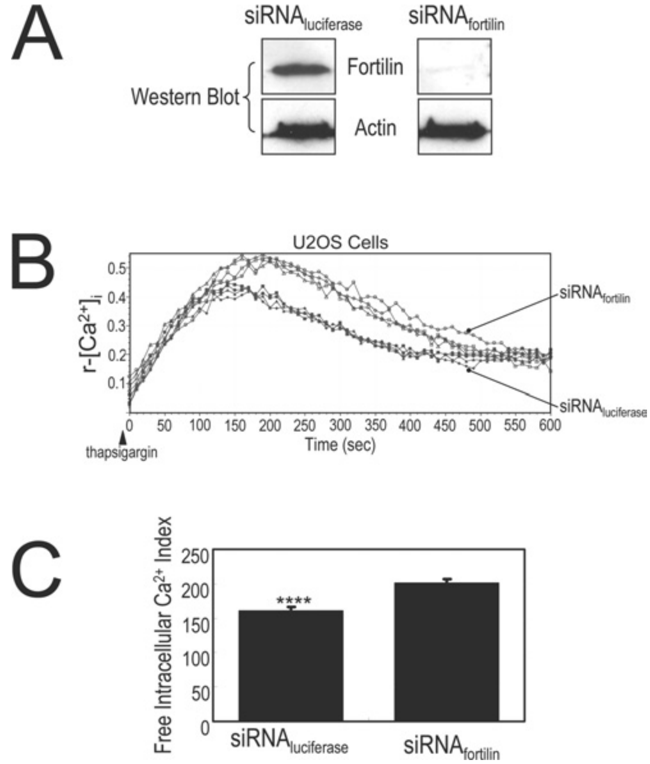

Figure 4 Fortilin blocks the thapsigargin-induced elevation of $[Ca^{2+}]_i$ in U2OS cells

(**A**) The treatment of U2OS cells with $siRNA_{fortilin}$ (siRNA against fortilin), but not $siRNA_{luciferase}$ (siRNA against luciferase, negative control), decreased cellular fortilin levels. (**B**) $[Ca^{2+}]_i$ of U2OS cells treated with either $siRNA_{fortilin}$ or $siRNA_{luciferase}$ upon thapsigargin challenge (400 nM). U2OS cells lacking fortilin ($siRNA_{fortilin}$) exhibit the exaggerated elevation of $[Ca^{2+}]_i$ in response to thapsigargin. See the Materials and methods section for experimental details. (**C**) Free intracellular Ca^{2+} index, the area under the curve, for U2OS cells treated with $siRNA_{luciferase}$, was significantly smaller than that for U2OS cells treated with $siRNA_{fortilin}$ [160 ± 5.7 and 201.5 ± 4.9 (arbitrary units) for cells treated with $siRNA_{luciferase}$ and $siRNA_{fortilin}$ respectively.]. ****$P < 0.001$.

siRNA depletion of fortilin augments the thapsigargin-induced increase in $[Ca^{2+}]_i$ in U2OS cells

To determine whether the presence of fortilin changes the intracellular Ca^{2+} concentration *in vivo*, we transfected U2OS cells with either $siRNA_{fortilin}$ or $siRNA_{luciferase}$. Treatment with $siRNA_{fortilin}$ reduced the intracellular fortilin concentration to undetectable levels ($siRNA_{fortilin}$, Figure 4A). Cells were then incubated in the presence of the Ca^{2+}-sensor dye Fura 2 and stimulated with thapsigargin to induce the release of Ca^{2+} from the ER into the cytosol. The r-$[Ca^{2+}]_i$ in both groups of U2OS cells increased rapidly after thapsigargin stimulation (Figure 4B). Strikingly, in this system, the r-$[Ca^{2+}]_i$ of $siRNA_{fortilin}$-treated U2OS cells increased significantly more than that of $siRNA_{luciferase}$-treated U2OS cells (Figures 4B and 4C). These results suggest that the presence of fortilin blunted the increase in $[Ca^{2+}]_i$ in thapsigargin-challenged U2OS cells.

$MEF_{fortilin+/-}$ with lower levels of fortilin exhibit a greater increase in $[Ca^{2+}]_i$ upon thapsigargin challenge than $MEF_{fortilin+/+}$

To determine whether our observation in thapsigargin-challenged U2OS cells was true in primary culture cells, we compared the r-$[Ca^{2+}]_i$ of thapsigargin-challenged $MEF_{fortilin+/-}$ and $MEF_{fortilin+/+}$. $MEF_{fortilin-/-}$ has not been successfully isolated. The fortilin expression level in $MEF_{fortilin+/-}$ was approx. half

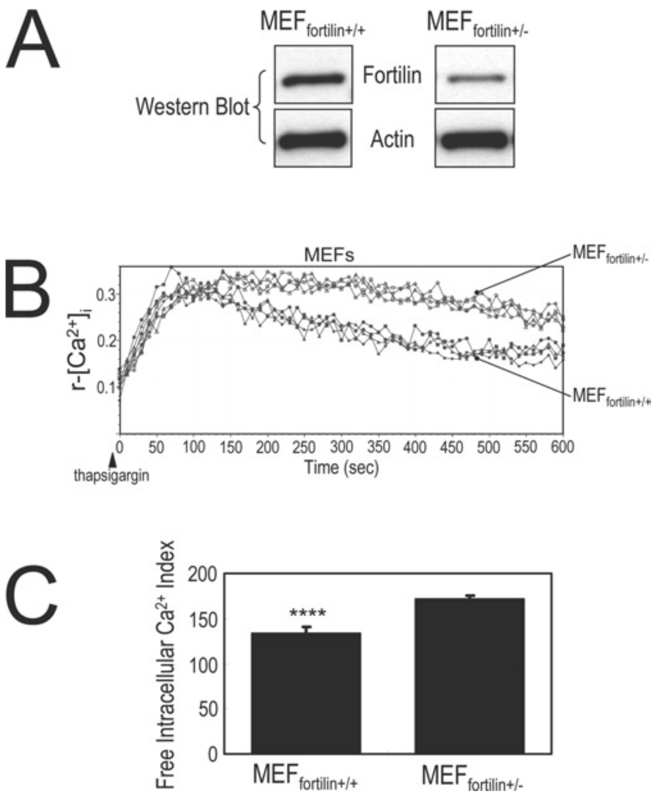

Figure 5 Fortilin blocks thapsigargin-induced elevation of free intracellular Ca^{2+} ($[Ca^{2+}]_i$) in MEF cells

(**A**) $MEF_{fortilin+/-}$ cells expressed a significantly smaller amount of intracellular fortilin than $MEF_{fortilin+/+}$ as measured by Western blot analysis. (**B**) r-$[Ca^{2+}]_i$ concentration of $MEF_{fortilin+/-}$ or $MEF_{fortilin+/+}$, upon thapsigargin challenge (400 nM). $MEF_{fortilin+/-}$ showed more exaggerated elevation of $[Ca^{2+}]_i$ to thapsigargin stimulation than did $MEF_{fortilin+/+}$. See the Materials and methods section for experimental details. (**C**) Free intracellular Ca^{2+} index, the area under the curve for $MEF_{fortilin+/+}$ cells was significantly smaller than that for $MEF_{fortilin+/-}$ cells (134.09 ± 6.4 arbitrary units and 172.1 ± 3.7 abitrary units for $MEF_{fortilin+/+}$ and $MEF_{fortilin+/-}$ cells respectively). $^{****}P < 0.001$.

that in $MEF_{fortilin+/+}$, as determined by Western blot analysis (Figure 5A). Upon thapsigargin challenge, $MEF_{fortilin+/-}$ exhibited a significantly higher r-$[Ca^{2+}]_i$ than did $MEF_{fortilin+/+}$ (Figures 5B and 5C). These results suggest that the presence of fortilin interfered with the thapsigargin-induced elevation of $[Ca^{2+}]_i$ in MEF. In our previous work [7], we demonstrated that fortilin is present in both the cytosol and the nucleus. In addition, thapsigargin has been shown to increase $[Ca^{2+}]_i$ by releasing Ca^{2+} that is stored in the ER into the cytosol [36,42,43]. Taken together, our present results suggest that fortilin scavenges Ca^{2+} released into the cytosol from the ER and blunts the elevation of $[Ca^{2+}]_i$ *in vivo*.

Fortilin blocks Ca^{2+}-dependent apoptosis in U2OS cells

To evaluate the biological consequence of fortilin-blunted $[Ca^{2+}]_i$ elevation in thapsigargin-challenged cells, we treated U2OS cells with either $siRNA_{fortilin}$ or $siRNA_{luciferase}$, stimulated them with thapsigargin in the presence or absence of the potent cell-membrane-permeant intracellular Ca^{2+} chelator BAPTA-AM, and then evaluated these cells for cell morphology (Figure 6A), cell death rate (Figure 6B) and for caspase 3 activation (Figure 6C). First, fortilin protected cells against thapsigargin-induced cell death because we observed far more rounded dead cells in $siRNA_{fortilin}$-treated cells that those treated by $siRNA_{luciferase}$ (Figure 6A; top panels) and because the EthD-1 index, representing the late phase of apoptosis or necrosis, was significantly higher in $siRNA_{fortilin}$-treated cells than in $siRNA_{luciferase}$-treated cells upon thapsigargin challenge (Figure 6B, column 1 compared with column 3; 5.10 ± 0.94 % compared with 1.65 ± 1.28 %; $^{**}P < 0.01$). Secondly, most of the cell death caused by the lack of fortilin was preventable by BAPTA-AM and therefore Ca^{2+}-dependent in nature. This was because the frequency of rounded dead cells in $siRNA_{fortilin}$-treated cells were reduced by BAPTA-AM almost to that in $siRNA_{luciferase}$-treated cells (Figure 6A, lower left-hand and upper right-hand panels respectively) and because most of cell death preventable by fortilin (indicated with #, Figure 6B) was preventable by BAPTA-AM and thus Ca^{2+}-dependent (Figure 6B). We then measured the caspase 3 activities of these cells. As shown in Figure 6(C), $siRNA_{fortilin}$-treated cells, but not $siRNA_{luciferase}$-treated cells, exhibited significant caspase 3 activation upon thapsigargin stimulation (1219 ± 359 compared

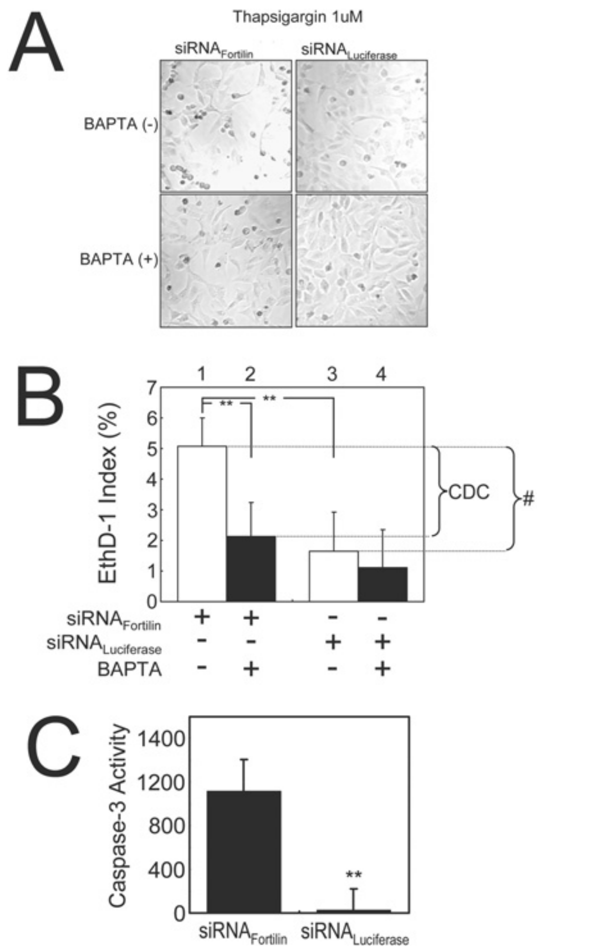

Figure 6 Fortilin inhibits thapsigargin-induced Ca^{2+}-dependent cell death in U2OS cells

(**A**) Morphology of BAPTA-AM-treated and -untreated U2OS cells transfected with either $siRNA_{fortilin}$ or $siRNA_{luciferase}$. BAPTA-AM-treatment reduces the percentage of dead cells (rounded and detached), especially in $siRNA_{fortilin}$-treated cells. Cell death preventable by BAPTA-AM (a potent Ca^{2+}-chelator), represented Ca^{2+}-dependent cell death. (**B**) Fortilin protected cells against thapsigargin-induced cell death (column 1 compared with column 3), most of which was Ca^{2+}-dependent cell death (CDC). $^{**}P < 0.01$; #, cell death blocked by fortilin. (**C**) The $siRNA_{fortilin}$-treated cells, but not $siRNA_{luciferase}$-treated cells, exhibit caspase 3 activation upon thapsigargin stimulation, suggesting that most of the cell death of $siRNA_{luciferase}$-treated cells in (**B**) (columns 3 and 4) represented necrosis (cell death lacking caspase 3 activation). $^{**}P < 0.01$.

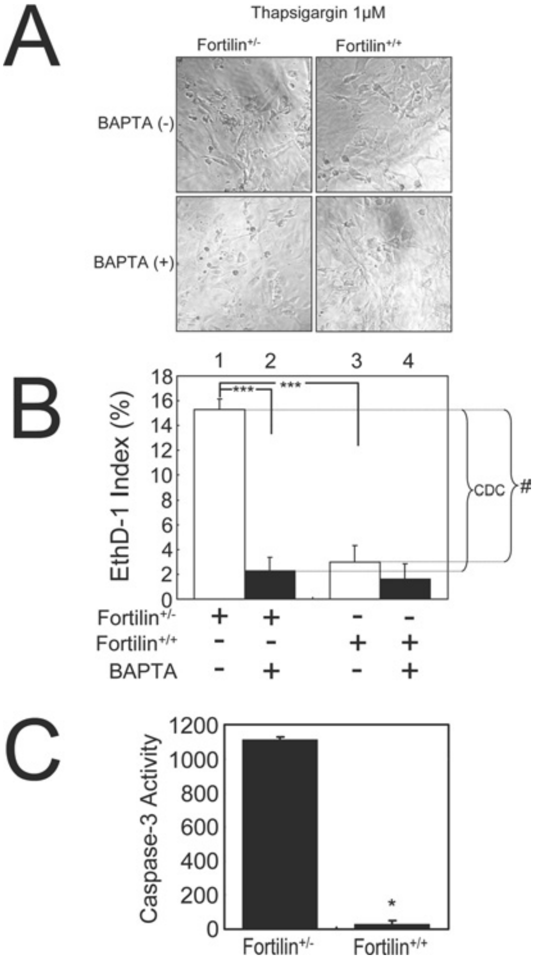

Figure 7 Fortilin inhibits thapsigargin-induced Ca^{2+}-dependent cell death in MEF cells

(**A**) Morphology of BAPTA-AM-treated and -untreated $MEF_{fortilin+/-}$ and $MEF_{fortilin+/+}$ cells. BAPTA-AM-treatment reduces the percentage of dead cells (rounded and detached), especially in $MEF_{fortilin+/-}$ cells. Cell death preventable by BAPTA-AM (a potent Ca^{2+}-chelator), represented Ca^{2+}-dependent cell death. (**B**) Fortilin protects cells against thapsigargin-induced, Ca^{2+}-mediated (BAPTA-AM-preventable), cell death (CDC). $^{***}P < 0.005$; #, cell death blocked by fortilin. (**C**) $MEF_{fortilin+/-}$ cells, but not $MEF_{fortilin+/+}$ cells, exhibit caspase 3 activation upon thapsigargin stimulation, suggesting that most of cell death of $MEF_{fortilin+/-}$ cells in (**B**) (columns 3 and 4) represented necrosis (cell death lacking caspase 3 activation). $^{*}P < 0.05$.

with 28 ± 213 relative units/μg of protein; $^{**}P < 0.01$). The absence of significant thapsigargin-induced caspase 3 activity in $siRNA_{luciferase}$-treated cells (Figure 6C, $siRNA_{luciferase}$) suggests that most of cell death of $siRNA_{luciferase}$-treated cells in Figure 6(B) (column 3) represented necrosis (cell death lacking caspase 3 activation). The results in turn suggest that most of BAPTA-AM-preventable cell death in $siRNA_{fortilin}$-treated cells is apoptosis. Taken together, the results presented in Figure 6 suggest that fortilin prevents the thapsigargin-induced elevation of $[Ca^{2+}]_i$ from inducing apoptosis in U2OS cells.

Fortilin blocks Ca^{2+}-dependent apoptosis in MEF cells

To determine whether the inhibition by fortilin of Ca^{2+}-dependent apoptosis seen in U2OS also occurs in primary culture cells, we compared the Ca^{2+}-dependent apoptosis rates in $MEF_{fortilin+/-}$ and $MEF_{fortilin+/+}$. MEF cells were stimulated with thapsigargin in the presence or absence of BAPTA-AM and evaluated for cell morphology (Figure 7A), cell death rate (Figure 7B) and caspase 3 activation (Figure 7C). Fortilin again protected cells against thapsigargin-induced cell death because we observed far more rounded dead cells in $MEF_{fortilin+/-}$ cells than in $MEF_{fortilin+/+}$ cells (Figure 7A, upper left-hand and upper right-hand panels respectively) and because the EthD-1 index was significantly higher in $MEF_{fortilin+/-}$ cells than in $MEF_{fortilin+/+}$ cells upon thapsigargin challenge (Figure 7B, column 1 compared with column 2; $15.28 \pm 2.0\,\%$ compared with $3.02 \pm 1.75\,\%$; $^{***}P < 0.005$). Secondly, most of the cell death caused by the lack of fortilin was again preventable by BAPTA-AM and therefore Ca^{2+}-dependent in nature. This was because the frequency of rounded dead $MEF_{fortilin+/-}$ cells were reduced by BAPTA-AM almost to that of rounded dead cells in $MEF_{fortilin+/+}$ (Figure 7A, lower left-hand and upper right-hand panels respectively) and because most of cell death preventable by fortilin (indicated by #, Figure 7B) was preventable by BAPTA-AM and thus Ca^{2+}-dependent (Figure 7B). We then measured the caspase 3 activities of these cells. As shown in Figure 7(C), $MEF_{fortilin+/-}$ cells, but not $MEF_{fortilin+/+}$ cells, exhibited significant caspase 3 activation upon thapsigargin stimulation (Figure 7C; 1110 ± 15.3 compared with 26 ± 22.5 relative units/μg of protein; $^{*}P < 0.05$). The absence of significant thapsigargin-induced caspase 3 activity in $MEF_{fortilin+/+}$ cells (Figure 7C, fortilin$^{+/+}$) suggests that most of the cell death of $MEF_{fortilin+/+}$ cells in Figure 7(B) (column 3) represented necrosis. The results also suggest that most of BAPTA-AM-preventable cell death in $MEF_{fortilin+/-}$ cells is apoptosis. Taken together, these results suggest that fortilin robustly protects MEFs against thapsigargin-induced apoptosis. Consistent with the data presented in Figure 6, the data presented in Figure 7 suggest that fortilin blocks the apoptosis resulting from thapsigargin-induced elevation of $[Ca^{2+}]_i$.

Glu^{58} and Glu^{60} of fortilin are critical for binding to Ca^{2+}

To determine what region(s) of fortilin are critical for Ca^{2+} binding, we synthesized 12 overlapping fortilin peptides (Figure 8A) and subjected them to equilibrium dialysis. As shown in Figure 8(B), CBB alone in the tube had the exact same radioactivity as CBB in the beaker (Buffer and thick line; Figure 8B). CBBs containing calmodulin, fortilin–His_6, and GST–fortilin were all significantly more radioactive than the CBB control (Figure 8B), consistent with the data presented in Figure 1(A). In this system, only three polypeptides, namely fortilin(43–62), fortilin(57–76) and fortilin(127–146), exhibited significantly more radioactivity than did the CBB control, suggesting that the binding of fortilin to Ca^{2+} occurred through amino acids within these three regions. There are eleven charged amino acids within these regions. We systematically mutated these charged amino acids to generate several mutants of full-length fortilin: fortilinΔ1 (D44A/D45A), fortilinΔ2 (E58A/E60A), fortilinΔ3 (E55A/E58A/E60A/E63A), fortilinΔ4 (D71A), fortilinΔ5 (E138A) and fortilinΔ6 (D143A) (Figure 9A). These six mutant proteins of fortilin were expressed as GST-fusion proteins, purified and characterized (Figure 9B) and subjected to the same equilibrium dialysis. In this experiment, the radioactivities of CBB-only and GST-only solutions were identical with the radioactivity of the CBB in the beaker (Buffer, GST-only; Figure 9C). As expected, calmodulin and GST–fortilin exhibited significantly more radioactivity than did CBB alone and GST-only (Figure 9C). In this system, the solutions containing GST–fortilinΔ5 and Δ6 were significantly more radioactive than the controls ($P < 0.005$ and $P < 0.05$ respectively), suggesting that neither Glu^{138} nor Asp^{143} played a critical role in the Ca^{2+} binding of fortilin (Figure 9C). Strikingly, however, the mutations introduced to Glu^{58} and Glu^{60} abolished

A

Name	Sequence
$Fortilin_{1-20}$	MIIYRDLISHDEMFSDIYKI
$Fortilin_{15-24}$	SDIYKIREIADGLCLEVEGK
$Fortilin_{29-48}$	LEVEGKMVSRTEGNIDDSLI
$Fortilin_{43-62}$	IDDSLIGGNASAEGPEGEGT
$Fortilin_{57-76}$	PEGEGTESTVITGVDIVMNH
$Fortilin_{71-90}$	DIVMNHHLQETSFTKEAYKK
$Fortilin_{85-104}$	KEAYKKYIKDYMKSIKGKLE
$Fortilin_{99-118}$	IKGKLEEQRPERVKPFMTGA
$Fortilin_{113-132}$	PFMTGAAEQIKHILANFKNY
$Fortilin_{127-146}$	ANFKNYQFFIGENMNPDGMV
$Fortilin_{141-160}$	NPDGMVALLDYREDGVTPYM
$Fortilin_{155-172}$	GVTPYMIFFKDGLEMEKC

B

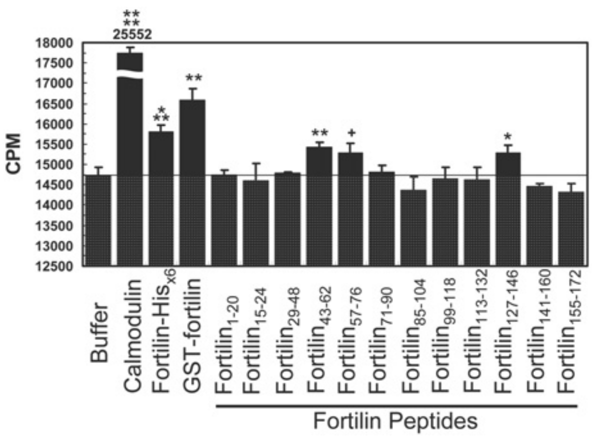

Figure 8 Short peptides of fortilin, fortilin(43–62), fortilin(57–76) and fortilin(127–146), bind Ca^{2+} in equilibrium dialysis assays

(**A**) Fortilin peptides covering various regions of fortilin were synthesized. Peptides in the highlighted rows are fortilin peptides that exhibited significant Ca^{2+}-binding activity in equilibrium dialysis assays. (**B**) Equilibrium dialysis of fortilin peptides showed significant binding of fortilin(43–62), fortilin(57–76) and fortilin(127–146) to Ca^{2+}. $^{****}P < 0.001$, $^{***}P < 0.005$, $^{**}P < 0.01$, $^{*}P < 0.05$, $^{+}P = 0.05$. CPM, counts per min.

almost completely the Ca^{2+}-binding capability of fortilin (GST–fortilinΔ2, Figure 9C). The finding that Glu^{58} and Glu^{60}, but not Glu^{138} or Asp^{143}, were critical to the Ca^{2+} binding of fortilin is entirely consistent with our finding in the Ca^{2+}-overlay assay that the 70 amino acid residues at the N-terminus of fortilin were critical for Ca^{2+} binding (Figure 1B). Based on these observations, we chose fortilinΔ2 to test the biological consequence of the inability of fortilin to bind Ca^{2+} *in vivo*. Intriguingly, the crystal structure of *Schizosaccharomyces pombe* fortilin (MMDB: 16785; PDB: 1H6Q) [44] shows that Glu^{58} and Glu^{60} were both localized in the loose loop of the molecule that protrudes from the surface of the more tightly packed portion of the molecule (Figure 9D).

FortilinΔ2(E58A/E60A), a fortilin point mutant lacking Ca^{2+}-binding activity, is more susceptible to thapsigargin-induced cell death than its wild-type counterpart

To establish that the protection by fortilin of thapsigargin-challenged cells against cell death is mediated via the binding of fortilin to Ca^{2+} and sequestration of Ca^{2+} from Ca^{2+}-dependent downstream apoptosis pathways, we established U2OS cell lines stably expressing wild-type fortilin ($U2OS_{fortilin\text{-}wild}$) and fortilinΔ2 ($U2OS_{fortilin\Delta2}$) as well as U2OS cells harbouring empty plasmids ($U2OS_{empty}$). Western blot analysis showed that exogenous fortilin and fortilinΔ2 were robustly expressed in $U2OS_{fortilin\text{-}wild}$ and $U2OS_{fortilin\Delta2}$ respectively (columns 2 and 3, Figure 10A). We then subjected these cell lines to thapsigargin and determined the EthD-1 indices. As expected, the EthD-1 index was significantly lower in $U2OS_{fortilin\text{-}wild}$ than it was in $U2OS_{empty}$ cells ($U2OS_{fortilin\text{-}wild}$ compared with $U2OS_{empty}$; 2.31 ± 0.57 % compared with 4.58 ± 0.39 % respectively; $^{*}P < 0.05$) (Fortilin compared with Empty, Figure 10B). Strikingly, the EthD-1 index of $U2OS_{fortilin\Delta2}$ cells was no different than that of $U2OS_{empty}$ cells ($U2OS_{fortilin\Delta2}$ compared with $U2OS_{empty}$; 3.96 ± 1.11 compared with 4.58 ± 0.39 % respectively; not significant) (FortilinΔ2 compared with Empty, Figure 10B). These results suggest that fortilin, but not fortilinΔ2, was capable of protecting cells against thapsigargin-induced cell death and that the ability of fortilin to bind Ca^{2+} was required for fortilin to protect cells against thapsigargin-induced cell death. Since most of the thapsigargin-induced cell death was Ca^{2+}-dependent (Figures 6B and 7B) and represented apoptosis (Figures 6C and 7C), it is suggested that the ability of fortilin to bind Ca^{2+} is required for fortilin to protect cells against Ca^{2+}-dependent apoptosis. These results further suggest that fortilin is a cytosolic Ca^{2+} scavenger and that anti-apoptotic activity of fortilin is at least partly due to its ability to sequester ER-derived Ca^{2+} from downstream Ca^{2+}-dependent apoptotic pathways.

DISCUSSION

For over a decade now, fortilin has been known to bind Ca^{2+} [8–12], but its biological significance has remained purely speculative. Since fortilin is an anti-apoptotic protein and Ca^{2+} plays a critical role in apoptosis, we hypothesized that fortilin binds and scavenges Ca^{2+}, thus preventing the ion from activating downstream apoptotic execution pathways. In the present study, we set out to test the hypothesis in a series of experiments. There are four key findings in the present study that are novel. First, we have employed four different assays, namely Ca^{2+}-overlay (Figure 1), flow dialysis (Figure 2), CD spectropolarimetry (Figure 3) and equilibrium dialysis (Figure 9C) assays to unequivocally demonstrate the presence of the binding of fortilin to Ca^{2+}. This was significant because previous studies relied entirely on Ca^{2+}-overlay assays to show the binding of fortilin to Ca^{2+} [8–12]. Importantly, the binding of fortilin to Ca^{2+} was associated with the change in secondary structure of fortilin as detected by CD spectropolarimetry (Figure 3). Secondly, we have been able to show, using both U2OS cells and MEFs and a standard Fura 2 Ca^{2+}-detection system, that the lack of fortilin led to an exaggerated elevation of free intracellular calcium levels ($[Ca^{2+}]_i$) upon thapsigargin stimulation (Figures 4 and 5). This is significant because it has not been reported previously that fortilin can block the elevation of $[Ca^{2+}]_i$ *in vivo*. Thirdly, we have demonstrated that fortilin protects cells against thapsigargin-induced Ca^{2+}-dependent apoptosis (Figures 6 and 7) and that the binding of fortilin to Ca^{2+} is required for fortilin's protection against such apoptosis (Figure 10), both of which have not been reported in the literature. Finally, we have identified amino acids of fortilin critical for its binding to Ca^{2+}, namely Glu^{58} and Glu^{60} and generated a double-point mutant of fortilin [fortilin(E58A/E60A) or fortilinΔ2] lacking Ca^{2+}-binding (Figure 9). Strikingly, wild-type fortilin, but not fortilin(E58A/E60A) (fortilinΔ2), protected cells against thapsigargin-induced cell death; fortilin is required to bind Ca^{2+} in order to block Ca^{2+}-dependent apoptosis. Based on these findings, we conclude the hypothesis above to be correct.

A

Name	Mutations
Fortilin Δ 1	$44^{D\to A}$, $45^{D\to A}$
Fortilin Δ 2	$58^{E\to A}$, $60^{E\to A}$
Fortilin Δ 3	$55^{E\to A}$, $58^{E\to A}$, $60^{E\to A}$, $63^{E\to A}$
Fortilin Δ 4	$71^{D\to A}$
Fortilin Δ 5	$138^{E\to A}$
Fortilin Δ 6	$143^{D\to A}$

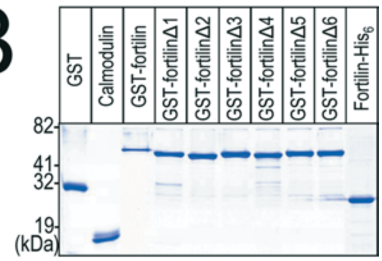

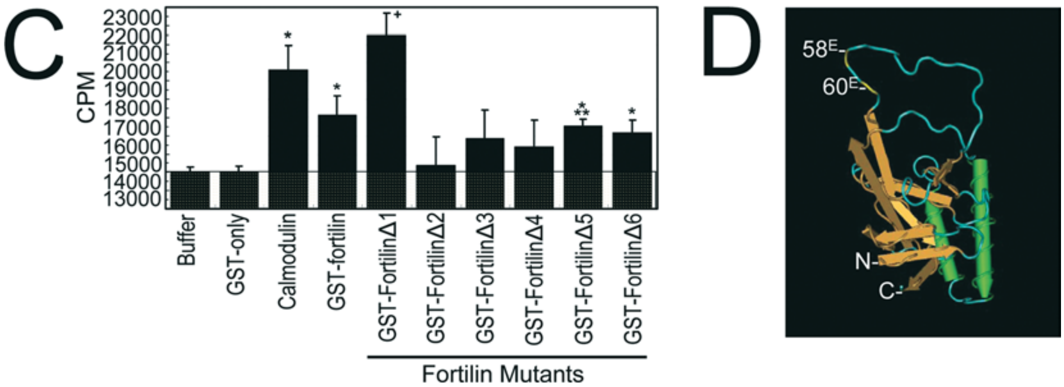

Figure 9 FortilinΔ2(E58A/E60A) fails to bind Ca^{2+} in equilibrium dialysis assays

(**A** and **B**) Generation and characterization of GST–fortilin mutants. Fortilin mutants containing point mutations within full-length fortilin, namely fortilinΔ1 (D44A/D45A), fortilinΔ2 (E58A/E60A), fortilinΔ3 (E55A/E58A/E60A/E63A), fortilinΔ4 (D70A), fortilinΔ5 (E138A) and fortilinΔ6 (D143A) (**A**), were generated, expressed with a GST-fusion tag, and characterized by SDS/PAGE and Coomassie Blue staining (**B**). The mutant in the yellow row (fortilinΔ2) exhibited significant Ca^{2+}-binding activity in equilibrium dialysis assays. (**C**) Equilibrium dialysis of GST–fortilin containing mutations showed the lack of significant binding by fortilinΔ2. $^{*}P < 0.05$, $^{+}P = 0.073$, $^{***}P < 0.005$. (**D**) Structure of *S. pombe* fortilin (PDB: 1H6Q) showing the localization of Glu^{58} and Glu^{60}. C, C-terminus; N, N-terminus.

Others besides ourselves have also tried to identify the Ca^{2+}-binding site of fortilin. Using fortilin–His_6 and fortilin fragments in a $^{45}Ca^{2+}$-overlay assay, Kim et al. [10] found that wild-type fortilin and fortilin(1–112), but not fortilin(1–80) or fortilin(1–52), bound $^{45}Ca^{2+}$. They therefore concluded that the Ca^{2+}-binding site of fortilin resides in amino acid residues 81–112. However, our experiments with GST–fortilin and its mutants suggest that the Ca^{2+}-binding site of fortilin resides in the polypeptide consisting of amino acids 1–70 (Figures 1B and 1C). In addition, our equilibrium dialysis assays showed no significant binding between Ca^{2+} and any of several fragments including fortilin(71–90), fortilin(85–104), fortilin(99–118) or fortilin(113–132) peptide. Furthermore, it did show very significant Ca^{2+} binding to fortilin(43–62) and fortilin(57–76) polypeptides (Figure 8). Consistently, there was no binding between Ca^{2+} and fortilinΔ2, a double-point mutant in which glutamate residues at amino acid positions 58 and 60 were mutated to alanine residues (Figure 9C). The apparent discrepancy between our findings and those of Kim et al. [10] may possibly be due to their use of fortilin(1–80), which carries a His_6-tag at its C-terminus and may not have folded properly. It is also possible that Glu^{58} and Glu^{60} consist in one of multiple Ca^{2+}-binding pockets within fortilin. The presence of at least two Ca^{2+}-binding pockets within fortilin is supported by our flow dialysis data presented in Figure 2. The co-crystallization data of fortilin and Ca^{2+} would allow us to determine the relative spatial contributions of these amino acid residues to Ca^{2+} and help to resolve this apparent discrepancy.

In the present study, flow dialysis assays provided a new insight into the binding of fortilin to Ca^{2+} where fortilin exhibited a biphasic Ca^{2+} binding (Figure 2), suggesting the presence of more than one, most probably two, high-affinity Ca^{2+}-binding sites, and the possible presence of multiple lower-affinity Ca^{2+}-binding sites. The high-affinity sites were almost saturated at approx. 8–18 μM Ca^{2+}, a finding consistent with CD spectropolarimetry data (Figure 3). Ca^{2+} binding to the lower-affinity sites seemed to disturb the measurement of the high-affinity sites and the Ca^{2+}-binding data to the latter were scattered. Although the high-affinity binding sites are likely to be responsible for the conformational change of fortilin observed in CD spectra (Figure 3), the exact nature of the Ca^{2+} binding to the low-affinity sites remains unclear. It is tempting to speculate that fortilin binds Ca^{2+} in a step-wise fashion *in vivo*: as the intracellular Ca^{2+} concentration ($[Ca^{2+}]_i$) starts to rise in response to apoptotic stimuli, fortilin binds and scavenges Ca^{2+}, using its higher-affinity Ca^{2+}-binding sites, to maintain $[Ca^{2+}]_i$ at a baseline level. The ligation of higher-affinity Ca^{2+}-binding sites may result in the conformational changes, as detectable by CD spectropolarimetry (Figure 3), to make lower-affinity Ca^{2+}-binding sites available for further Ca^{2+} binding. Nevertheless, the exact biological role of lower-affinity Ca^{2+}-binding sites calls for further biochemical studies.

Several groups of investigators have also investigated the link between the thapsigargin-induced increase in $[Ca^{2+}]_i$ and apoptosis. Thastrup et al. [45] showed that thapsigargin induces rapid and dose-dependent release of stored Ca^{2+} from ER-rich microsomes, resulting in a robust increase in $[Ca^{2+}]_i$, and that thapsigargin does so by inducing the acute and highly specific arrest of SERCA in the ER and consequent rapid leakage of Ca^{2+} into the cytosol [45]. Srivastava et al. [46] demonstrated that $[Ca^{2+}]_i$ elevation is the primary mechanism that thapsigargin uses

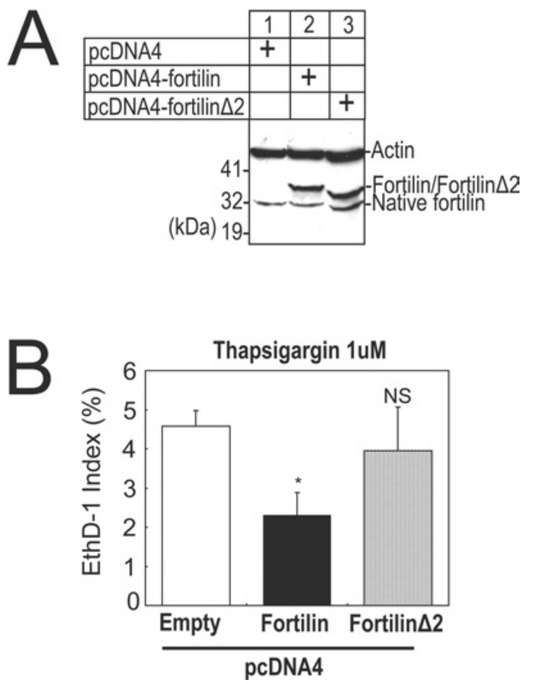

Figure 10 FortilinΔ2 (E58A/E60A), a non-Ca^{2+}-binding mutant of fortilin, fails to prevent thapsigargin-induced cell death

(**A**) Western blot analysis of U2OS cells. Actin, loading control; Native fortilin, fortilin natively expressed in U2OS cells, Fortilin/fortilinΔ2, over-expressed fortilin or fortilinΔ2(E58A/E60A) detected by an anti-fortilin antibody. (**B**) EthD-1 indices of U2OS cells stably harbouring empty plasmid (Empty), stably expressing wild-type fortilin (Fortilin) and stably expressing fortilinΔ2(E58A/E60A)(FortilinΔ2). $^*P < 0.05$ in comparison with Empty; NS, no statistically significant difference in comparison with Empty. The overexpression of fortilin, but not fortilinΔ2, a non-Ca^{2+}-binding mutant of fortilin, protects cells against thapsigargin-induced cell death.

to induce apoptosis by showing that the ability of thapsigargin to induce apoptosis was effectively blocked by buffering $[Ca^{2+}]_i$ with BAPTA-AM [46]. They also observed that $[Ca^{2+}]_i$ elevation was associated not only with the release of cytochrome *c* from mitochondria but also with caspase 3 activation [46]. In the present study, we consistently observed that BAPTA-AM drastically reduced the rate of cell death in both fortilin-deficient cells (U2OS cells treated with $siRNA_{fortilin}$ and $MEF_{fortilin+/-}$) and control cells, suggesting the majority of thapsigargin-induced cell death is Ca^{2+}-dependent. Importantly, thapsigarin-induced cell death in $siRNA_{luciferase}$-treated cells and $MEF_{fortilin+/+}$ (column 3 of Figures 6 and 7) was not associated with caspase activation (Figures 6C and 7C), suggesting that EthD-1 positivity in these cells represented necrosis, rather than apoptosis. In that light, most of the cell death blocked by the presence of fortilin was both Ca^{2+}-dependent and apoptotic in nature. Strikingly, fortilin(E58A/E60A) (fortilinΔ2), a double-point mutant of fortilin lacking Ca^{2+}-binding activity, was not capable of protecting cells against thapsigargin-induced cell death (Figure 10). It follows that the binding of fortilin to Ca^{2+} is required if fortilin is to function as an anti-apoptotic agent in thapsigargin-induced, Ca^{2+}-dependent apoptosis. In addition, the difference seen in the indices of EthD-1 for control samples among experiments (Figures 6 and 10) most probably represents the fact that U2OS cells used in Figure 6 were treated with $siRNA_{luciferase}$, whereas $U2OS_{empty}$ cells used in Figure 10 had been stably transfected with pcDNA4-empty plasmid vector. It is thus safe to conclude that the primary mechanism by which fortilin blocks thapsigargin-induced Ca^{2+}-dependent apoptosis is through its binding to Ca^{2+}. In future investigations of possible roles of fortilin in Ca^{2+}-independent apoptosis, a double-point mutant fortilin(E58A/E60A) will prove to be a highly effective reagent.

The present study was supported in part by grants from the NIH (National Institutes of Health; HL04015 and HL68024) (to K. F.), the Roderick Duncan MacDonald General Research Fund at St. Luke's Episcopal Hospital (to K. F.) and the Royal Golden Jubilee Graduate Program of Thailand Research Fund (PhD/0200/2545 to P. G.; PhD/0200/2685 to M. T.) and by an Established Investigator Award from the American Heart Association (to K. F.).

REFERENCES

1 Zhang, D., Li, F., Weidner, D., Mnjoyan, Z. H. and Fujise, K. (2002) Physical and functional interaction between MCL1 and fortilin. The potential role of MCL1 as a fortilin chaperone. J. Biol. Chem. **277**, 37430–37438
2 Kozopas, K. M., Yang, T., Buchan, H. L., Zhou, P. and Craig, R. W. (1993) MCL1, a gene expressed in programmed myeloid cell differentiation, has sequence similarity to BCL2. Proc. Natl. Acad. Sci. U.S.A. **90**, 3516–3520
3 Li, F., Zhang, D. and Fujise, K. (2001) Characterization of fortilin, a novel anti-apoptotic protein. J. Biol. Chem. **276**, 47542–47549
4 Zhang, C., Cai, Y., Adachi, M. T., Oshiro, S., Aso, T., Kaufman, R. J. and Kitajima, S. (2001) Homocysteine induces programmed cell death in human vascular endothelial cells through activation of the unfolded protein response. J. Biol. Chem. **276**, 35867–35874
5 Sturzenbaum, S. R., Kille, P. and Morgan, A. J. (1998) Identification of heavy metal induced changes in the expression patterns of the translationally controlled tumour protein (TCTP) in the earthworm *Lumbricus rubellus*. Biochim. Biophys. Acta **1398**, 294–304
6 Tuynder, M., Susini, L., Prieur, S., Besse, S., Fiucci, G., Amson, R. and Telerman, A. (2002) Biological models and genes of tumor reversion: cellular reprogramming through tpt1/TCTP and SIAH-1. Proc. Natl. Acad. Sci. U.S.A. **99**, 14976–14981
7 Graidist, P., Phongdara, A. and Fujise, K. (2004) Antiapoptotic protein partners fortilin and MCL1 independently protect cells from 5-FU-induced cytotoxicity. J. Biol. Chem. **279**, 40868–40875
8 Haghighat, N. G. and Ruben, L. (1992) Purification of novel calcium binding proteins from *Trypanosoma brucei*: properties of 22-, 24- and 38-kilodalton proteins. Mol. Biochem. Parasitol. **51**, 99–110
9 Sanchez, J. C., Schaller, D., Ravier, F., Golaz, O., Jaccoud, S., Belet, M., Wilkins, M. R., James, R., Deshusses, J. and Hochstrasser, D. (1997) Translationally controlled tumor protein: a protein identified in several nontumoral cells including erythrocytes. Electrophoresis **18**, 150–155
10 Kim, M., Jung, Y., Lee, K. and Kim, C. (2000) Identification of the calcium binding sites in translationally controlled tumor protein. Arch. Pharm. Res. **23**, 633–636
11 Rao, K. V., Chen, L., Gnanasekar, M. and Ramaswamy, K. (2002) Cloning and characterization of a calcium-binding, histamine-releasing protein from *Schistosoma mansoni*. J. Biol. Chem. **277**, 31207–31213
12 Arcuri, F., Papa, S., Carducci, A., Romagnoli, R., Liberatori, S., Riparbelli, M. G., Sanchez, J. C., Tosi, P. and del Vecchio, M. T. (2004) Translationally controlled tumor protein (TCTP) in the human prostate and prostate cancer cells: expression, distribution, and calcium binding activity. Prostate **60**, 130–140
13 Xu, A., Bellamy, A. R. and Taylor, J. A. (1999) Expression of translationally controlled tumour protein is regulated by calcium at both the transcriptional and post-transcriptional level. Biochem. J. **342**, 683–689
14 Hajnoczky, G., Davies, E. and Madesh, M. (2003) Calcium signaling and apoptosis. Biochem. Biophys. Res. Commun. **304**, 445–454
15 Wang, X. (2001) The expanding role of mitochondria in apoptosis. Genes Dev. **15**, 2922–2933
16 Fladmark, K. E., Brustugun, O. T., Mellgren, G., Krakstad, C., Boe, R., Vintermyr, O. K., Schulman, H. and Doskeland, S. O. (2002) Ca^{2+}/calmodulin-dependent protein kinase II is required for microcystin-induced apoptosis. J. Biol. Chem. **277**, 2804–2811
17 Tan, K. M., Chan, S. L., Tan, K. O. and Yu, V. C. (2001) The *Caenorhabditis elegans* sex-determining protein FEM-2 and its human homologue, hFEM-2, are Ca^{2+}/calmodulin-dependent protein kinase phosphatases that promote apoptosis. J. Biol. Chem. **276**, 44193–44202
18 Kruidering, M., Schouten, T., Evan, G. I. and Vreugdenhil, E. (2001) Caspase-mediated cleavage of the Ca^{2+}/calmodulin-dependent protein kinase-like kinase facilitates neuronal apoptosis. J. Biol. Chem. **276**, 38417–38425
19 Aagaard-Tillery, K. M. and Jelinek, D. F. (1995) Differential activation of a calcium-dependent endonuclease in human B lymphocytes. Role in ionomycin-induced apoptosis. J. Immunol. **155**, 3297–3307
20 Blanchard, H., Grochulski, P., Li, Y., Arthur, J. S., Davies, P. L., Elce, J. S. and Cygler, M. (1997) Structure of a calpain Ca^{2+}-binding domain reveals a novel EF-hand and Ca(2+)-induced conformational changes. Nat. Struct. Biol. **4**, 532–538

21 Lin, G. D., Chattopadhyay, D., Maki, M., Wang, K. K., Carson, M., Jin, L., Yuen, P. W., Takano, E., Hatanaka, M., DeLucas, L. J. and Narayana, S. V. (1997) Crystal structure of calcium bound domain VI of calpain at 1.9 Å resolution and its role in enzyme assembly, regulation, and inhibitor binding. Nat. Struct. Biol. **4**, 539–547

22 Mandic, A., Viktorsson, K., Strandberg, L., Heiden, T., Hansson, J., Linder, S. and Shoshan, M. C. (2002) Calpain-mediated Bid cleavage and calpain-independent Bak modulation: two separate pathways in cisplatin-induced apoptosis. Mol. Cell Biol. **22**, 3003–3013

23 Wang, H. G., Pathan, N., Ethell, I. M., Krajewski, S., Yamaguchi, Y., Shibasaki, F., McKeon, F., Bobo, T., Franke, T. F. and Reed, J. C. (1999) Ca^{2+}-induced apoptosis through calcineurin dephosphorylation of BAD. Science **284**, 339–343

24 Teubl, M., Groschner, K., Kohlwein, S. D., Mayer, B. and Schmidt, K. (1999) Na^{+}/Ca^{2+} exchange facilitates Ca^{2+}-dependent activation of endothelial nitric-oxide synthase. J. Biol. Chem. **274**, 29529–29535

25 Fujise, K., Zhang, D., Liu, J. and Yeh, E. (2000) Regulation of apoptosis and cell cycle progression by MCL1. Differential role of proliferating cell nuclear antigen. J. Biol. Chem. **275**, 39458–39465

26 Gong, L., Kamitani, T., Fujise, K., Caskey, L. S. and Yeh, E. T. (1997) Preferential interaction of sentrin with a ubiquitin-conjugating enzyme, Ubc9. J. Biol. Chem. **272**, 28198–28201

27 Guo, H., Mockler, T., Duong, H. and Lin, C. (2001) SUB1, an *Arabidopsis* Ca^{2+}-binding protein involved in cryptochrome and phytochrome coaction. Science **291**, 487–490

28 Yazawa, M. (2002) Quantitative analysis of Ca^{2+}-binding by flow dialysis. Methods Mol. Biol. **173**, 3–14

29 Mishra-Gorur, K., Singer, H. A. and Castellot, Jr, J. J. (2002) Heparin inhibits phosphorylation and autonomous activity of Ca^{2+}/calmodulin-dependent protein kinase II in vascular smooth muscle cells. Am. J. Pathol. **161**, 1893–1901

30 Florian, J. A. and Watts, S. W. (1998) Integration of mitogen-activated protein kinase kinase activation in vascular 5-hydroxytryptamine2A receptor signal transduction. J. Pharmacol. Exp. Ther. **284**, 346–355

31 Hsieh, C. C. and Lau, Y. (1998) Migration of vascular smooth muscle cells is enhanced in cultures derived from spontaneously hypertensive rat. Pflugers Arch. **435**, 286–292

32 Elbashir, S. M., Lendeckel, W. and Tuschl, T. (2001) RNA interference is mediated by 21- and 22-nucleotide RNAs. Genes Dev. **15**, 188–200

33 Elbashir, S. M., Harborth, J., Lendeckel, W., Yalcin, A., Weber, K. and Tuschl, T. (2001) Duplexes of 21-nucleotide RNAs mediate RNA interference in cultured mammalian cells. Nature **411**, 494–498

34 Heinrich, J. N., O'Rourke, E. C., Chen, L., Gray, H., Dorfman, K. S. and Bravo, R. (1994) Biological activity of the growth factor-induced cytokine N51: structure–function analysis using N51/interleukin-8 chimeric molecules. Mol. Cell. Biol. **14**, 2849–2861

35 Lytton, J., Westlin, M. and Hanley, M. R. (1991) Thapsigargin inhibits the sarcoplasmic or endoplasmic reticulum Ca-ATPase family of calcium pumps. J. Biol. Chem. **266**, 17067–17071

36 Foyouzi-Youssefi, R., Arnaudeau, S., Borner, C., Kelley, W. L., Tschopp, J., Lew, D. P., Demaurex, N. and Krause, K. H. (2000) Bcl-2 decreases the free Ca^{2+} concentration within the endoplasmic reticulum. Proc. Natl. Acad. Sci. U.S.A. **97**, 5723–5728

37 Spencer, J. P., Rice-Evans, C. and Williams, R. J. (2003) Modulation of pro-survival Akt/protein kinase B and ERK1/2 signaling cascades by quercetin and its *in vivo* metabolites underlie their action on neuronal viability. J. Biol. Chem. **278**, 34783–34793

38 Shi, Q., Chen, H. L., Xu, H. and Gibson, G. E. (2005) Reduction in the E2K subunit of the α-ketoglutarate dehydrogenase complex has effects independent of complex activity. J. Biol. Chem. **280**, 10888–10896

39 Furukawa, R., Maselli, A., Thomson, S. A., Lim, R. W., Stokes, J. V. and Fechheimer, M. (2003) Calcium regulation of actin crosslinking is important for function of the actin cytoskeleton in *Dictyostelium*. J. Cell Sci. **116**, 187–196

40 Furuyama, T. and Dzelzkalns, V. A. (1999) A novel calcium-binding protein is expressed in *Brassica pistils* and anthers late in flower development. Plant Mol. Biol. **39**, 729–737

41 Lee, B. I., Mustafi, D., Cho, W. and Nakagawa, Y. (2003) Characterization of calcium binding properties of lithostathine. J. Biol. Inorg. Chem. **8**, 341–347

42 Jiang, S., Chow, S. C., Nicotera, P. and Orrenius, S. (1994) Intracellular Ca^{2+} signals activate apoptosis in thymocytes: studies using the Ca^{2+}-ATPase inhibitor thapsigargin. Exp. Cell Res. **212**, 84–92

43 Lam, M., Dubyak, G., Chen, L., Nunez, G., Miesfeld, R. L. and Distelhorst, C. W. (1994) Evidence that BCl-2 represses apoptosis by regulating endoplasmic reticulum-associated Ca^{2+} fluxes. Proc. Natl. Acad. Sci. U.S.A. **91**, 6569–6573

44 Thaw, P., Baxter, N. J., Hounslow, A. M., Price, C., Waltho, J. P. and Craven, C. J. (2001) Structure of TCTP reveals unexpected relationship with guanine nucleotide-free chaperones. Nat. Struct. Biol. **8**, 701–704

45 Thastrup, O., Cullen, P. J., Drobak, B. K., Hanley, M. R. and Dawson, A. P. (1990) Thapsigargin, a tumor promoter, discharges intracellular Ca^{2+} stores by specific inhibition of the endoplasmic reticulum Ca^{2+}-ATPase. Proc. Natl. Acad. Sci. U.S.A. **87**, 2466–2470

46 Srivastava, R. K., Sollott, S. J., Khan, L., Hansford, R., Lakatta, E. G. and Longo, D. L. (1999) Bcl-2 and Bcl-X(L) block thapsigargin-induced nitric oxide generation, c-Jun NH_2-terminal kinase activity, and apoptosis. Mol. Cell. Biol. **19**, 5659–5674

Received 22 May 2007/30 July 2007; accepted 17 August 2007
Published as BJ Immediate Publication 17 August 2007, doi:10.1042/BJ20070679